

Probabilistic Evaluation of Liquefaction Spread for Lifeline Structures

Ikuo Katayama¹⁾, J. A. Pires²⁾ and A. H.-S. Ang²⁾

ABSTRACT

Using Monte Carlo simulation, the probability of liquefaction in a soil layer spreading over a finite area is calculated. Vertical propagation of seismic wave and horizontally layered soil are assumed for random vibration analysis. Statistical spatial correlation of the undrained shear strength of sand against liquefaction is considered with perfectly correlated input ground motion excitation characterized by power spectrum and peak factor. The fragility curves against liquefaction spread of finite strips extending along lifelines with specified levels of base input ground motions for typical sand layers of Metropolitan Tokyo are presented.

1. Introduction

The authors have been developing a probabilistic analysis method of liquefaction of layered soil under random seismic loads[1].

The method has been applied to evaluate the seismic reliability of the connectivity of electric power transmission network of a small area of Metropolitan Tokyo. The reliability of the connectivity of an example low voltage power network was found to be strongly degraded by the presence of liquefaction of the sand layers within which the pipes were buried at shallow depth[2].

It was assumed that an area of 500 m x 500 m would totally liquefy when the soil profile representing the soil properties of the above unit area showed the possibility of liquefaction against a given ground acceleration, that the hume-pipes for power transmission buried within the area would be damaged somewhere within the area and that when damage of the pipes due to liquefaction should occur the power cables installed therein would be cut off without exception causing electrical disconnection.

This assumption was adopted, because there is no information about the behavior of buried hume-pipes under liquefaction; however, the assumption

1) Tokyo Electric Power Services Co., Ltd., Tokyo, Japan

2) Department of Civil Engineering, University of California, Irvine, U.S.A.

seems reasonable for discussing electrical disconnectivity. The authors have extended their work in two areas: one is to estimate the strength of soil after liquefaction and its interaction with buried pipes[3]; the other is to probabilistically estimate the lateral liquefaction spread within an area which has liquefied[4].

The last work is comprehensively discussed in J.A. Pires et al[5]; however, there we discussed only the case where a finite area will liquefy and contiguously spread with decreasing probability in all directions.

When we apply our results to a practical case of liquefaction of soil surrounding buried power cable ducts of low voltage, lifelines that are closest to demands, we should consider the practical situation of these pipes: due to installation of a pipe underground, the surrounding soil might have been disturbed, and with the work and the existence of the pipe underground water will collect along the pipe that may extend several hundred meters for various configurations. Therefore, the liquefied area of the surrounding soil may collectively spread along the pipe more than in the other directions; such damages as uplift of manholes and heaving-up of the buried pipes along the path of pipes due to liquefaction have been observed in recent past earthquakes.

In this paper, not only to estimate the proximity of liquefaction along the buried structure but also to estimate the magnitude of the area along the buried structures where restoration work may be necessary after liquefaction, the probability of contiguous soil liquefaction spread along a finite longitudinal strip is discussed.

2. Liquefaction Analysis Model

2.1 Cyclic Resistance Curves against Liquefaction

The resistance of sand against liquefaction is defined by the number of cycles, $N_f(\bar{\tau})$, of constant amplitude shear stress ratio, $\bar{\tau}$, necessary to induce liquefaction known as "cyclic resistance curve". The load term, the shear stress ratio, is defined as τ/σ'_{v0} , where τ is the working stress in the soil and σ'_{v0} is the effective overburden stress. Based on the occurrence of liquefaction during past earthquakes, the cyclic stress ratios have been correlated with Standard Penetration Test Blowcount normalized to an effective overburden stress of 1.0 ton/ft² and an energy ratio of 60%, $(N)_{60-SPT}$ [6].

Based on the above observed correlation between $(N)_{60-SPT}$ and the stress ratio, τ/σ'_{v0} , the authors derived such "cyclic resistance curves against liquefaction" as is shown in Fig. 1 with different fine contents for Magnitude 7.5 earthquake. The detail of the process to obtain the curves is given in J.A. Pires

et al[1].

2.2 Random Seismic Loading

Any of the "cyclic resistance curves" can be interpreted by

$$N_f(\bar{\tau})[E_c(\bar{\tau})h(\bar{\tau})] = W_u \quad (1)$$

where W_u is an arbitrary constant, $E_c(\bar{\tau})$ is the energy dissipated through hysteresis in one cycle of shear stress amplitude $\bar{\tau}$, and $h(\bar{\tau})$ is a weighing function. The concept of the number of equivalent uniform loading cycles implies that under N loading cycles with different shear stress, $\bar{\tau}_i$, liquefaction will occur when

$$W = \sum_{i=1}^N E_c(\bar{\tau}_i) h(\bar{\tau}_i) \quad (2)$$

reaches W_u .

The probability that liquefaction will occur at any point in the critical layer of a layered soil, independently of liquefaction occurring anywhere else in the layer, is given by

$$P[E_0] = \int_0^{\infty} F_{W_u}(q) f_{W(a,t)}(q) dq \quad (3)$$

where F_{W_u} denotes the PDF of W_u and $f_{W(a,t)}$ is the probability density function of $W(a,t)$.

For an earthquake with a given intensity $A=a$, and a strong motion duration $T_g=t$, liquefaction occurs when

$$Z = W_u - W(a,t) < 0.0 \quad (4)$$

where W_u denotes the hysteretic energy dissipation capacity of the soil layer and if this capacity is exhausted the liquefaction will set up. The quantity $W(a,t)$ is given by

$$W(a,t) = \int_0^t X(r) \dot{\epsilon}_{\tau}(r) dr \quad (5)$$

where $\dot{\epsilon}_{\tau}(\tau)$ is the rate of hysteretic energy dissipated at time r and $X(r)$ is an equivalent weighing function to include the effect of random stress

amplitude[7],

$$X(r) = \left[\int_0^{\bar{\tau}_m} h(\bar{\tau}) E_c(\bar{\tau}) f_T(\bar{\tau}, r) d\bar{\tau} \right] / \left[\int_0^{\bar{\tau}_m} E_c(\bar{\tau}) f_T(\bar{\tau}, r) d\bar{\tau} \right] \quad (6)$$

where $\bar{\tau}_m$ is the normalized maximum of the hysteretic component of the shear stress for the sand and $f_T(\bar{\tau}, r)$ is the probability density function of the peaks of $\bar{\tau}$ at time r .

The mean and variance of $W(a, t)$ are obtained from random vibration analysis [7,8].

On the other hand, the statistics of W_u are obtained from the uncertainty analysis of the cyclic resistance against liquefaction and the "cyclic resistance curves" in Figs. 1(a) to 1(c), are regarded as the mean resistance curves and the coefficient of variation(c.o.v.) was found to be 0.57 for a given *N-SPT blowcount* by assuming independence of the stress ratio to cause liquefaction[1]. When the uncertainties in the *N-SPT blowcount* are considered, the c.o.v. of the *N-SPT blowcount* will increase. Considering the c.o.v. of 0.15 for the *N-SPT blowcount*, the c.o.v. of approximately 0.8 for the number of uniform loading cycles till liquefaction is used in our study.

2.3 Response Analysis of the Layered Soil

The total shear strain at each layer of the liquefiable layer defined by $\dot{\gamma}_i = (x_{i+1} - x_i) / \Delta h_i$ is calculated by idealizing the soil layer as a multi-degree of freedom lumped mass model with viscous damper at the bottom with the outcrop input ground motion defined at the top of the base layer; where x_i and Δh_i denote the total response displacement of the mass i and the thickness of the i -th layer, respectively. A hysteretic model and an analytical procedure[7,9,10] are used here to represent the soil hysteresis and calculate the necessary component of the shear stress by a first-order differential equation. Statistical linearization is used in the solution of the nonlinear equation.

The hysteretic component, z , of the shear strain is expressed by

$$\frac{\partial z}{\partial \gamma} = A - \beta \frac{|z|}{\dot{\gamma}} |z|^{r-1} - \delta |z|^r \quad (7)$$

where γ is the total shear strain, A, β, δ and r are parameters that describe the shape of the hysteresis loop. Then the shear stress is given by

$$\tau = \alpha G_m \gamma + (1 - \alpha) G_m z \quad (8)$$

where G_m is the initial shear modulus and αG_m is the residual stiffness. The maximum hysteretic shear stress is then given by

$$\tau_m = (1 - \alpha) G_m [A / (\beta + \delta)]^{1/r} \quad (9)$$

In this study, the following values are used for the smooth hysteretic model:

Assuming $r=0.5$ in Eq.(7) and the Hardin-Drnevich type strain-dependency curve is assumed with the reference strain $\gamma_r=4.0 \times 10^{-4}$, respectively. Also the following parameters are used:

$$A=1.0, \quad \delta = \beta, \quad \alpha = 0.05$$

with β and γ calculated from Eq.(9) for a specified value of τ_m .

2.4 Input Ground Motion Statistics

In the analysis, the stochastic input ground motion is characterized by a stationary Gaussian random process; power spectral density function defined by Clough-Penzien[11].

$$S(\omega) = S_0 \frac{1 + 4\zeta_B^2 (\omega/\omega_B)}{[1 - (\omega/\omega_B)^2 + 4\zeta_B^2 (\omega/\omega_B)^2]} \frac{(\omega/\omega_G)^4}{[1 - (\omega/\omega_G)]^2 + 4\zeta_G^2 (\omega/\omega_G)^2} \quad (10)$$

where the parameters $\omega_B = 16.9 \text{ rad/s}$, $\zeta_B = 0.94$, $\zeta_G = 0.7$, and $\omega_G = 1.25 \text{ rad/s}$ were chosen. This ground motion is applied at the hypothetical outcrop surface of the base layer.

2.5 Calibration of the method

In order to assess the reliability of the above method, the probabilities of liquefaction were computed for some past case histories of occurrence or non-occurrence of liquefaction. The case histories investigated are summarized in Table 1. Cases 1, 3, 4, 6, 9B, 9T, 10 and 11 were investigated. The results of the investigation are shown in Fig. 2. The line shown in Fig. 2 separates the data for which liquefaction has occurred from those data for which liquefaction has not occurred for Magnitude 7.5 earthquakes. The probability of the onset of liquefaction computed with the methodology appear to be consistent with the

observed data.

3. Lateral Extent of Liquefaction Spread

3.1 Methodology

The probability that liquefaction will occur at any point in the critical layer of a particular layered soil has been given by the previous Eq.(3). The soil resistance capacity and the load terms, respectively W_u and $W(a, t)$, are replaced by S and Q here, to simplify the description.

The soil resistance in a finite area, $B \times L$, of concern is described by a two-dimensional homogeneous lognormal random process with mean \bar{S} , variance σ_s^2 and auto-correlation function of resistance capacity $R_{SS}(r_{ij})$, where r_{ij} is the horizontal distance between any two points in the layer. The area is divided into elementary squares with side D numbered $i=1,2,\dots,N$, as shown in Fig. 3.

The soil resistance against liquefaction at the center of the elementary squares are random variables denoted by S_i , $i=1,2,\dots,N$. Here, within the elementary square, the probability of liquefaction is assumed to be kept unchanged from the value given to the layer. Then the random variables S_i are identically distributed but are not statistically independent. The coefficient of correlation for a pair of random variables (S_i, S_j) is

$$\rho_{SS}(r_{ij}) = \frac{R_{SS}(r_{ij})}{\sigma_{S_i} \sigma_{S_j}} \quad (11)$$

where $\sigma_{S_i} = \sigma_{S_j} = \sigma_S$.

The probability that liquefaction will extend over the entire area $B \times L$ is the probability that all elements within that area will liquefy. Therefore,

$$P_L(B, L) = [(S_1 < Q) \cap (S_2 < Q) \cap \dots \cap (S_N < Q)] \quad (12)$$

which can be written as

$$P_L(B, L) = \int_0^{\infty} F_{S_1, \dots, S_N}(q, \dots, q) f_Q(q) dq, \quad (13)$$

where

$$F_{S_1, \dots, S_N}(q, \dots, q) = \int_0^q \dots \int_0^q f_{(S_1, \dots, S_N)}(S_1, \dots, S_N) dS_1 \dots dS_N \quad (14)$$

The integral in Eq.(13) for each value of q is evaluated using Monte Carlo

simulation. Here, it is assumed that the input ground motion defined at the base layer is perfectly correlated within the area $B \times L$. The practical computation is performed after transforming both the variables S_i and Q (see [5]).

3.2 Contiguous Lateral Spread in All Direction

The examples of liquefaction fragilities at any point within the area of concern for soil deposits B and F, the soil profiles of which are shown in Fig. 4, are shown in Fig. 5[5]. For these deposits, the correlation function

$$\rho_{S,S}(r) = \exp[-(r/b)^2] \quad (15)$$

is applied for generating two-dimensional homogeneous horizontally correlated random field. In the equation, b is a positive parameter called correlation coefficient and r is the horizontal distance between any two points in the layer.

Various methods have been proposed to estimate the parameter b for the correlation function of soil properties[12,13]. The correlation length defines a distance such that the average number of uncorrelated observations of the soil property within it is 1.0. The value b in Eq.(15) is converted from the correlation length δ_u as $b = \delta_u / \sqrt{\pi}$ and ranges from about 30 m to 40 m. The actual values of b should be evaluated for a particular case as the adverse consequences of liquefaction will depend on the size of contiguous liquefaction relative to the diameter of the buried pipes and manholes. In this paper, however, the liquefaction fragilities for soil deposit F with was computed by making the size of squared-area $B=L$ as parameter; e.g., let B from 1.94 to 5.81 times b . Therefore, if we assume $b=40$ m, then $B=L$ becomes about 80 m to 230 m.

The results are shown in Fig. 6; the probability of liquefaction contiguously spreading over a given area decreases very rapidly as the area increases. Fig.7 shows another expression of the probability of contiguous liquefaction with the size of squared-areas.

Using the proposed method it is also possible to compute the probabilities that a specified fraction of the area $B \times L$ will liquefy[14]. The method is also possible to be directly applied to estimate the probability of liquefaction spread along a finite strip where long pipes are assumed to be buried in shallow depth.

3.3 Contiguous Longitudinal Spread in a Strip

The proposed method was applied assuming rectangular-area as shown in Fig. 8. The soil deposits selected are the previous F and B, and further E of which soil profile is shown in Fig. 9. These soil deposits are very popular in

Metropolitan Tokyo.

First, the liquefaction fragilities for soil deposits F, E and B are shown in Fig. 11. Among them the results for soil deposits F and B are the same with those given in the previous Fig. 5 even if they were separately computed and the results for soil deposit E is newly added.

Taking width B and Length L of a rectangular-area in Fig. 8 as 40 and 500 m, respectively, the proposed method was directly applied to the above three types of deposits to estimate the probability of liquefaction spread along a finite strip where long pipes or ducts are assumed to be buried in shallow depth. The results are shown in Fig. 11. The size of element area was chosen as 20 m x 62.5 m and the correlation coefficient as $b=62.4$ m which may give more adverse consequences in spreading the liquefaction along the area of concern than the case using the reported values of b ranging from 30 m to 40 m.

The probability of liquefaction contiguously spreading over a given strip also decreases as the area increases.

For comparison, if we take the previous results for soil deposit F from the case with the base peak acceleration, $PGA=0.095$ g and lateral extent of liquefaction $L=6$ (actual squared-area has $L=B= 62.4$ m x 5.81 = 363 m), the probability of contiguous liquefaction spread in the squared-area becomes about 0.35, whereas the corresponding result of this time, the probability of contiguous liquefaction spread along the strip, becomes 0.5 by taking $L_s/L=363$ m/500 m = 0.725 and the interpolated result at $PGA=0.95$ from those of PGAs 0.090 and 0.098 in Fig. 11. It seems reasonable to obtain more adverse result from the case of spread along a finite strip than the previous case of squared-area.

4. Discussion

As we already pointed out, when we consider the practical situation of soil surrounding buried pipes, due to installation of a pipe underground, the surrounding soil might have been disturbed and, with the work and the existence of the pipe, underground water will collect along the pipe that may extend several hundred meters for various configurations. Therefore, the liquefied area of the surrounding soil may collectively spread along the pipe more than in the other directions; such damages as uplift of manholes and heaving-up of the buried pipes along the path of pipes due to liquefaction have been observed in recent past earthquakes. The proposed method to evaluate lateral liquefaction spread of layered soil deposits has given reasonable results numerically as already shown in the preceding part of this paper.

Based upon the results above obtained, the proposed method seems to give us more useful and practical information in the evaluation of seismic reliability of power transmission network as follows:

Fig. 12 shows a model electric network located in Metropolitan Tokyo and the probability of black-out at the demand nodes of 66 kv in 25 years[2]. The location of the area of concern is plotted in Fig. 13(a) denoted as "C" and the Annual Probability of Exceedance of PGA at the location is given in Fig. 13(b). The higher values of probability of black-out (electrical disconnectivity just after an earthquake) for demand nodes are distributed within and near the hatched meshes which have been evaluated as the meshes very vulnerable to liquefaction. This is considered reasonable because these meshes are lying on old river bed or terrace.

It was assumed that an area (a mesh) of 500 m x 500 m would totally liquefy when the soil profile representing soil properties of the above unit area showed the possibility of liquefaction against a given ground acceleration, that the hume-pipes for power transmission buried within the area would be damaged somewhere within the area and that when damage of the pipes due to liquefaction should occur the power cables installed therein would be cut off without exception causing electrical disconnection.

This assumption was adopted, because there is no information about the behavior of buried hume-pipes under liquefaction and the assumption seems reasonable for discussing electrical disconnectivity; however, as already shown in the previous Figs. 7 and 11, the probability of liquefaction contiguously spreading over a given area decreases very rapidly as the area or the length of strip increases.

The hatched meshes in Fig. 12 consist of soil deposits 3, 4 and 6 shown in Fig. 14. Among them, soil-3 and soil-4 respectively corresponds to soil F and E in this study. The probabilities of liquefaction for these soil deposits are given in Table 2. Although it is not clear how the structural consequences due to liquefaction will be affected by the size of liquefaction spread along the structures, however, it may be reasonable to estimate severer damage for larger liquefaction spread but with less probability.

From the demand node distribution of the model network, hume-pipes for power transmission have around 250 m unit-length.

The expected PGA for 25 year-return period is 0.18 g at the ground surface evaluated as 0.12 g at the base layer[2], and the annual probability of exceedance of PGA at the location C is 0.25 from Figs. 13(a) and 13(b). The probabilities of liquefaction for soils F and E are 0.99 and 0.38 from Fig. 11. Therefore, the probability of liquefaction spreading contiguously over this length for each soil deposit will become $1-2.6 \times 10^{-3}$ and 9.1×10^{-1} , respectively; as similar to the results shown in Table 3. However, if we take the full length of the pipes within a mesh, it becomes $1-5.2 \times 10^{-3}$ and 0.08, respectively for soils F and E; in this case the decrease of the contiguous liquefaction probability is remarkable for soil deposit E (soil-6).

The above information obtained here may be helpful in planning the

restoration work and formation of work force for local power supply network after damaging earthquakes.

From the above results, it should be emphasized that since larger the value b becomes, the probability of contiguous liquefaction extending over a particular area or finite strip will become larger, the value b should be evaluated for a particular project; the adverse consequences of liquefaction will depend on the lateral extent of contiguous liquefaction relative to the diameter of the buried pipes and manholes. Also in this regards, the relation between the lateral extent of liquefaction and the practical consequences of buried structures should be extensively investigated.

5. Conclusion

A method to calculate the probability of the onset of liquefaction in horizontally layered soil deposits as a function of the expected maximum ground acceleration is presented. The method are practically consistent with past observed case histories of on-occurrence or non-occurrence of liquefaction.

The method was extended to compute the probability that liquefaction will spread over a given squared-area and a finite strip where lifelines are buried. It was observed that the probability of liquefaction spreading over a given area decreases as the contiguous lateral extent of liquefaction increases.

The method was applied to re-evaluate the vulnerability of a model power transmission network of Metropolitan Tokyo to liquefaction. The results may help future study on not only the seismic assessment of buried lifelines but also on the restoration planning by relevant organizations.

References

- [1] J.A. Pires, A.H.-S. Ang, and I. Katayama, Probabilistic analysis of liquefaction, in : Structural Dynamics and Soil Structure Interaction, eds. A.S. Cakmak and I Herrera(Computational Mechanics Publications, England, 1989), pp.155-168.
- [2] Ikuo Katayama, Ikumasa Yoshida, and Hitoshi Nakase, Reliability of electric power transmission systems in seismically active Metropolitan Tokyo, in Parts.1 to 3, Proceedings, ICOSSAR '89, pp.693-716.
- [3] J.A. Pires, H.-S. Ang, I. Katayama and M. Satoh, Post-liquefaction soil-structure interaction for buried structures: Sensitivity studies, Proc., SMIRT-12, MK02/4(K. Kusmaul(Editor), 1993 Elsevier Science Publishers), pp.225-230.
- [4] J.A. Pires, A.H.-S. Ang, and I. Katayama, Probabilistic evaluation of lateral

- liquefaction spread under earthquake loading, Proc., ICOSSAR'93 (Structural Safety & Reliability, Shueller, Shinozuka & Yao(eds), 1994 Balkema), pp.2009-2015.
- [5] J.A. Pires, A.H-S. Ang, and I. Katayama, Probabilistic evaluation of lateral extent of soil liquefaction under earthquake loading, Nuclear Engineering and Design 147, 1994, pp.157-170.
- [6] H.B. Seed et al, The influence of SPT procedures in soil liquefaction evaluation, Report No. UCB/EERC-84/15, University of California, Berkeley California (Oct., 1984)
- [7] J.A. Pires, Y.K. Wen, and A.H.-S. Ang, Stochastic analysis of liquefaction under earthquake loading, Struct. Res. Series, 504, University of Illinois Urbana, Illinois(April, 1983).
- [8] J.A. Pires and M. Tang, Statistics of hysteretic energy dissipated under random dynamic loading, J. Engrg. Mech., ASCE, 116(8) (1990) pp.1706-1722
- [9] Y.K. Wen, Equivalent linealization for hysteretic systems under random excitation, J.Appl.Mech., Transactions, ASME, 47(1)(1980), pp.150-154.
- [10] T.T. Baber and Y.K. Wen, Random vibration of hysteretic degrading multistory structures, J. Engrn. Mech., ASCE, 107(6)(1981), pp. 1069-1087
- [11] Ray W. Clough and Joseph Penzien, Dynamics of structures (McGraw-Hill: New York, 1975), pp.613-615.
- [12] N.M. Fardis and D. Veneziano, Estimation of SPT-N and relative density, J.Geotech. Engrg., ASCE, 107(10) (1981) pp.1345-1359.
- [13] E.H. Vanmarcke, Probabilistic modeling of soil profiles, J. Geotech. Engrg., ASCE, 103(11) (1977) pp.1227-1246.
- [14] M. Hoshiya, Probability of liquefaction spread, in:Stochastic Structural Dynamics 2 - New Practical Applications, eds. I. Elishakoff, Y.K. Lin(Springer-Verlag, Heidelberg, 1991) pp.45-54.

Table 1 Pertinent Data for the Case Histories Analyzed
(Cases 1,3,5,6,9_B,9_T and 11)

Case History	Date	Site	M	Distance (Miles)	T_k (sec)	a_{max}	Depth of Water Table (ft)	D (ft)	σ'_{vo} (pcf)	N-SPT	N_L	$\frac{\gamma_{ave}}{\sigma'_{vo}}$	Field Behavior	Reference
1	1964	Niigata	7.5	32	8	0.17	3	20	1200	7	10	0.195	Liq.	Seed and Idriss (1967)
2	1964	Niigata	7.5	32	8	0.17	3	25	1500	15	18	0.195	Liq.	Kishida (1966)
3	1964	Niigata	7.5	32	8	0.17	3	20	1200	9	14	0.195	No-Liq.	Seed and Idriss (1967)
4	1964	Niigata	7.5	32	8	0.17	12	25	2000	6	6	0.12	No-Liq.	Seed and Idriss (1967)
5	1968	Hachinohe	7.8	45-100	15	0.21	3	12	800	14	22	0.23	No-Liq.	Ohsaki (1970)
6	1968	Hachinohe	7.8	45-100	15	0.21	3	12	800	4	6	0.23	Liq.	Ohsaki (1970)
7	1968	Hachinohe	7.8	45-100	15	0.21	5	10	800	15	23	0.105	No-Liq.	Ohsaki (1970)
8	1968	Hakodate	7.8	100	15	0.21	3	15	1000	6	9	0.205	Liq.	Kishida (1970)
9 _U	1968	Hachinohe	7.8	45-100	15	0.21	7	47	2900	25	18	0.19	No-Liq.	Ohsaki (1970)
9 _T	1968	Hachinohe	7.8	45-100	15	0.21	7	9	850	16	23	0.16	No-Liq.	Ohsaki (1970)
10	1802	Niigata	6.6	24	8	0.12	3	20	1200	12	14	0.135	No-Liq.	Seed and Idriss (1967)
11	1807	Niigata	6.1	29	8	0.08	3	20	1200	9	14	0.09	No-Liq.	Seed and Idriss (1967)

Table 2 Parameters of Equivalent Lognormal Distribution for the Fragility Curves for Liquefaction

Soil Profile	(cm/s ²)					
	1	2	3	4	5	6
Median	297.0	1240.0	72.1	102.0	418.0	105.0
Log Std. Dev.	0.24	0.44	0.20	0.22	0.38	0.18

Table 3 Probabilities of Liquefaction for Six Soil Profiles

Soil Profile Probability	1	2	3	4	5	6
Annual	1.6×10^{-3}	3.4×10^{-6}	2.5×10^{-1}	1.1×10^{-1}	7.9×10^{-4}	9.6×10^{-2}
25 years	3.9×10^{-2}	8.5×10^{-5}	1.76×10^{-4}	9.4×10^{-1}	2.0×10^{-2}	9.2×10^{-1}
50 years	7.7×10^{-2}	1.7×10^{-4}	1.56×10^{-7}	1.34×10^{-3}	3.9×10^{-2}	1.65×10^{-3}

$$P_{fn} = 1 - (1 - P_{f1})^n$$

where : P_{fn} = probability in n years
 P_{f1} = annual probability

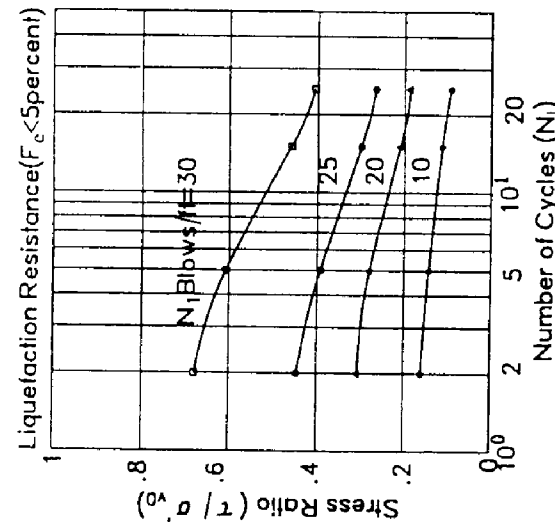
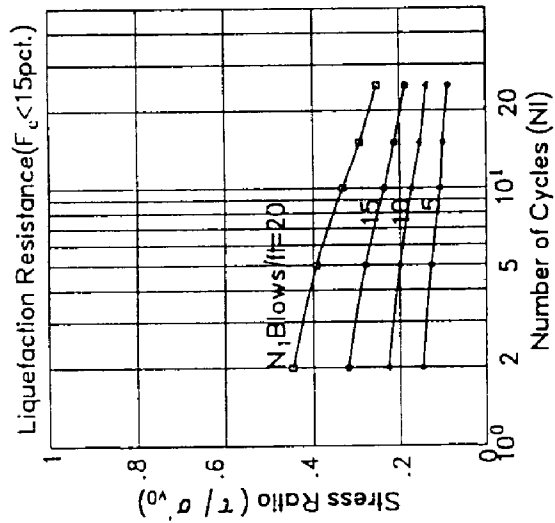
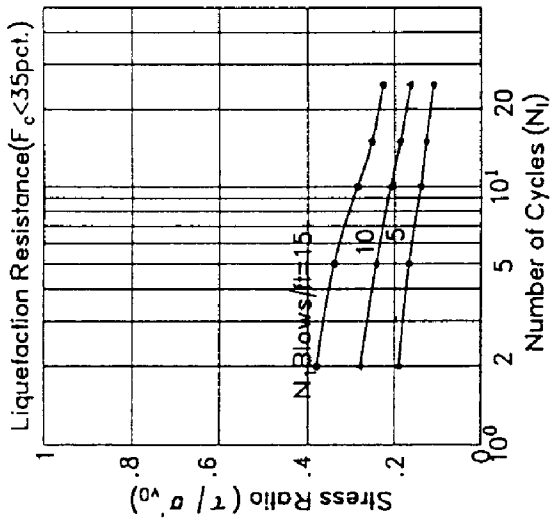


Fig. 1 Cyclic resistance curves against liquefaction for different Fine contents

CALCULATED PROBABILITIES

CASE HISTORY	PROBABILITY	CASE HISTORY	PROBABILITY
1	1.000	9 _B	0.233
3	0.954	9 _T	0.000026
5	0.460	10	0.142
6	1.000	11	0.000058

● — LIQUEFACTION OBSERVED ○ — LIQUEFACTION NOT OBSERVED

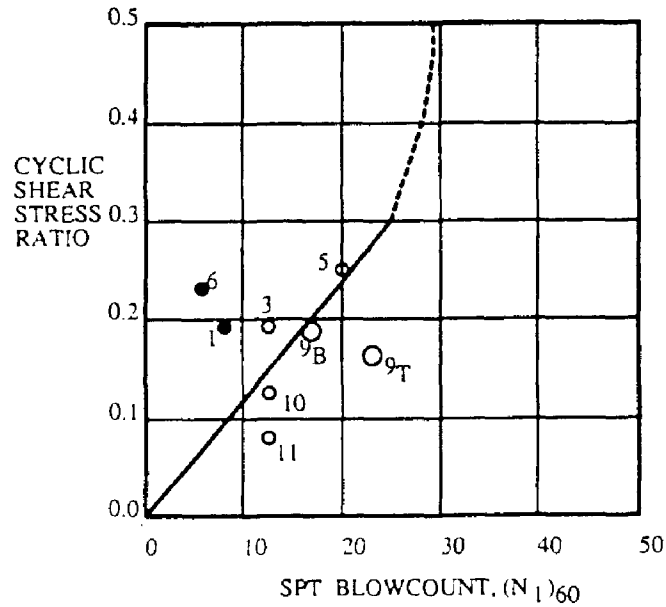


Fig. 2 Probabilities of liquefaction for selected case-histories.

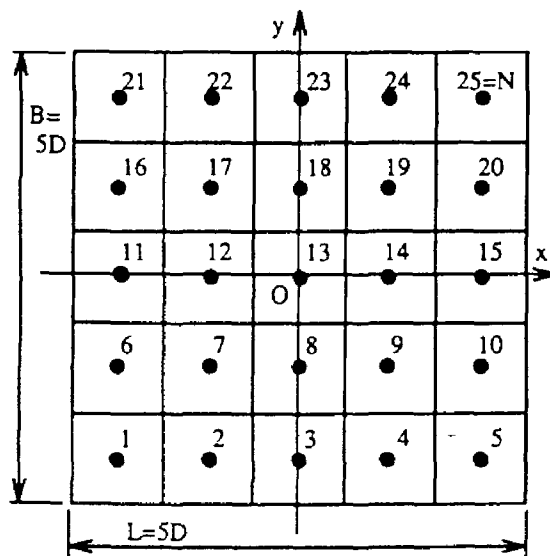


Fig. 3 Discretization of area $B \times L$ into elementary squared-areas.

DEPTH (m)	SOIL TYPE	N-SPT Uncorrected	SHEAR WAVE VELOCITY (m/sec)	PERCENT FINES
Water Table 3.0				
7.0	LOAM	4	160	—
12.0	LOAM with CLAY	5	173	—
17.0	CLAYED SAND	22	225	32
23.0	SILT	18	263	—
		>50	>450	

(a)

(m) G L	Name of Layer	N - SPT	Shear Wave Velocity (m/sec)	Fc (%)
0.5m	Upper Yurakucho Formation (sand)	10	175	21
6.0	Lower Yurakucho Formation (clayed-sand)	3	119	44
11.0		>50	>450 m/sec	

(b)

Fig. 4 Soil deposits analyzed:(a) soil B; (b) soil F

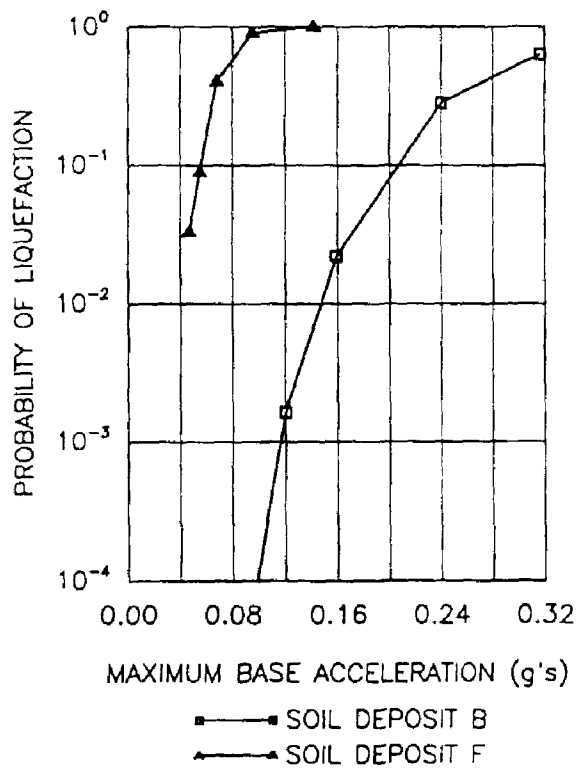


Fig. 5 Liquefaction fragilities for soil deposits B and F.

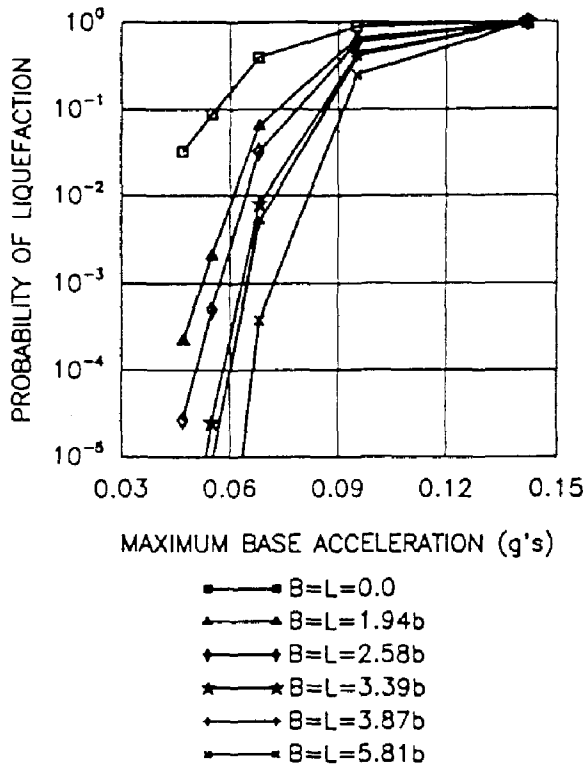


Fig. 6 Liquefaction fragilities soil deposits F

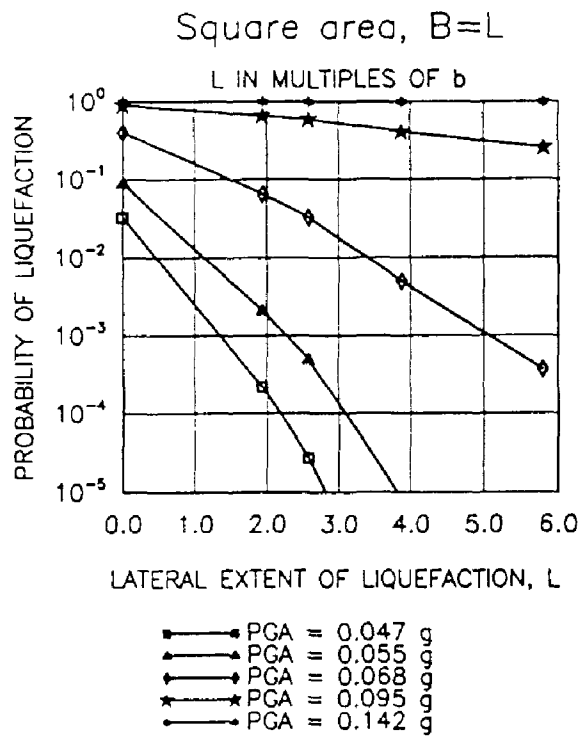


Fig. 7 Probability of liquefaction spreading in the layer (soil deposit F).

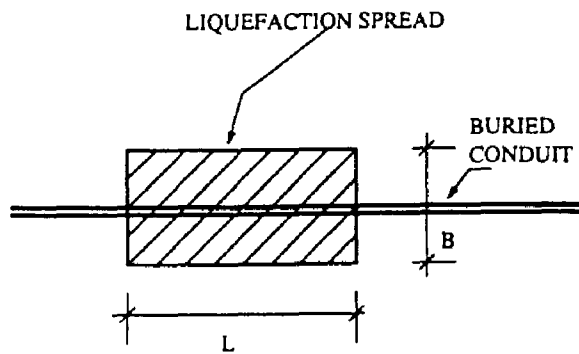


Fig. 8 Liquefaction spread along buried conduit.

Depth (m)	Name of Layer	N SPT *	Shear Wave Velocity (m/sec)	Percent Fines
0.5	Upper Yurakucho (SAND)	10	175	21
5.0				
*UNCORRECTED		>50	>450	--

Fig. 9 Soil profile of soil deposit E

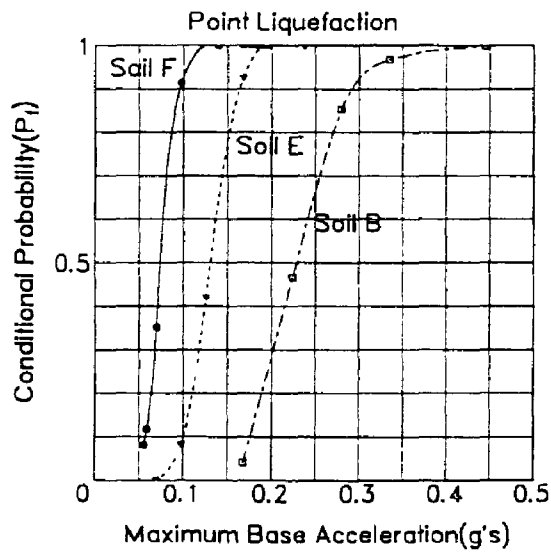


Fig.10 Probabilities of liquefaction for soil deposits analyzed

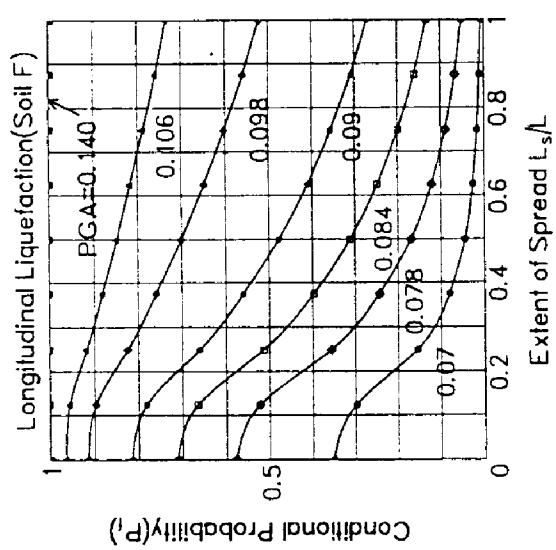
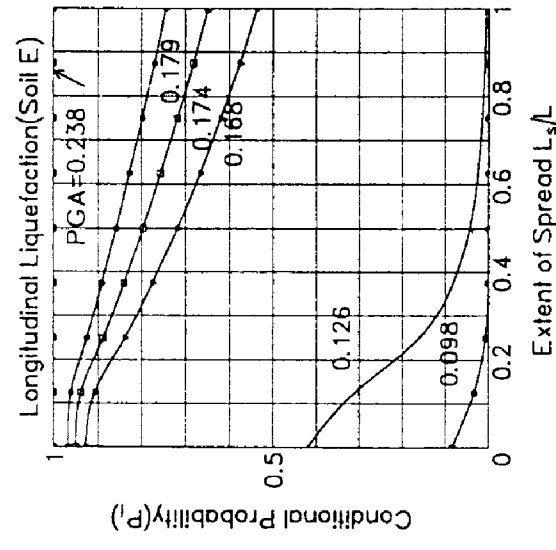
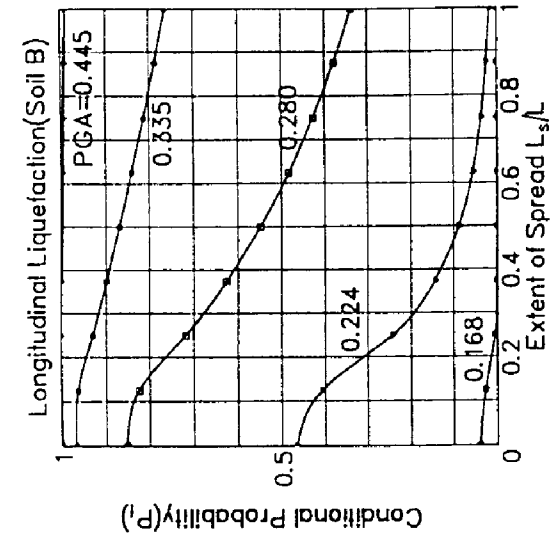
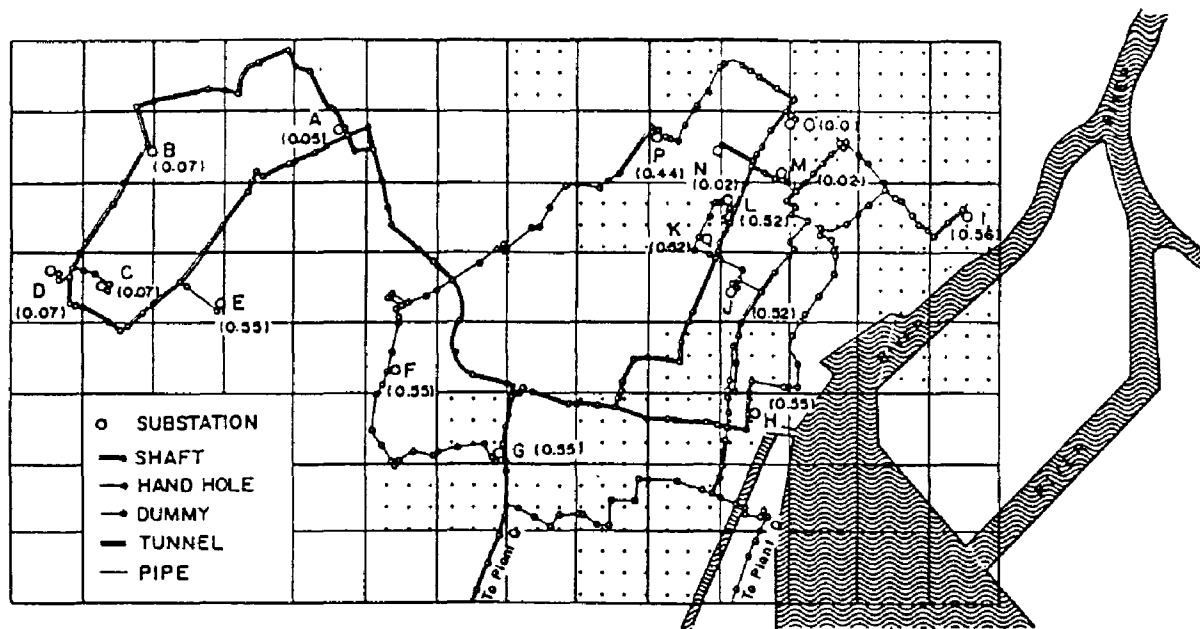


Fig.11 Probabilities of liquefaction for soil deposits analyzed




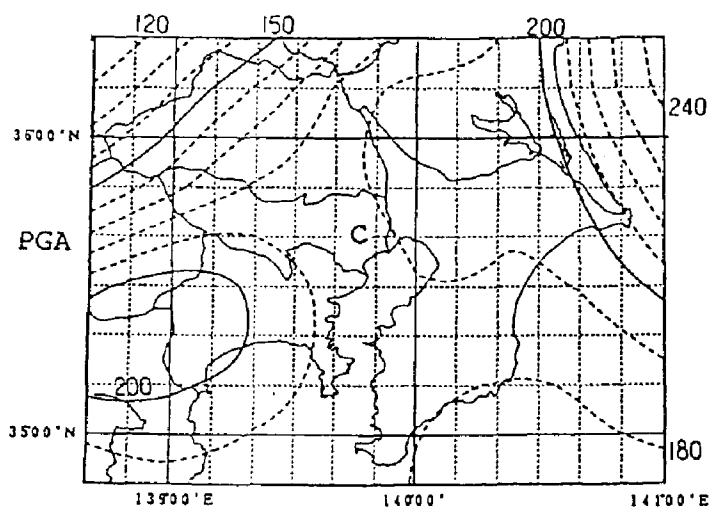
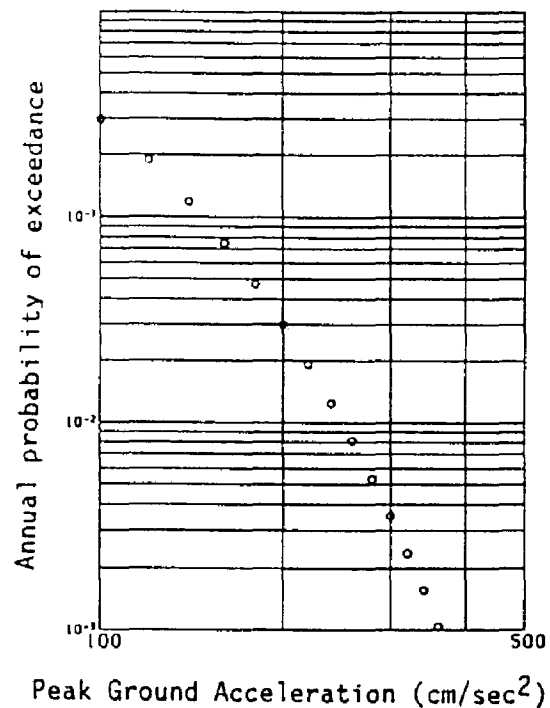
 : Hatched meshes correspond to soil profiles 3, 4 and 6 which are easy to liquefy.

Fig.12 Model Electric Network and Probabilities of Black-Out at the Demand Nodes of 66 kv in 25 Years



(a)



(b)

Fig.13 Expected acceleration for 25 year return period(a) and annual probability of exceedance of PGA at C(b)

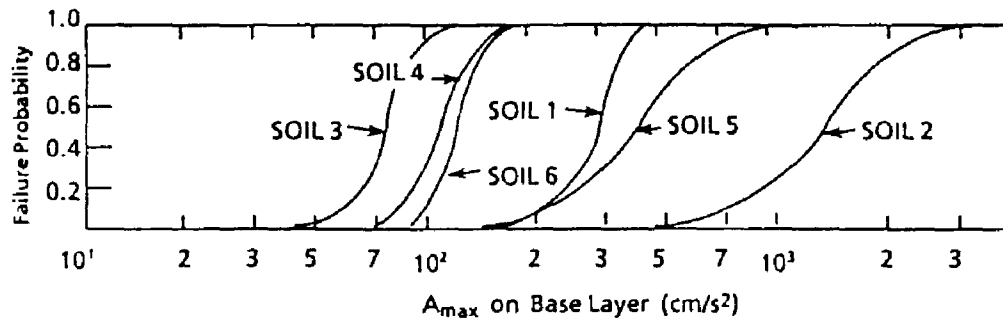
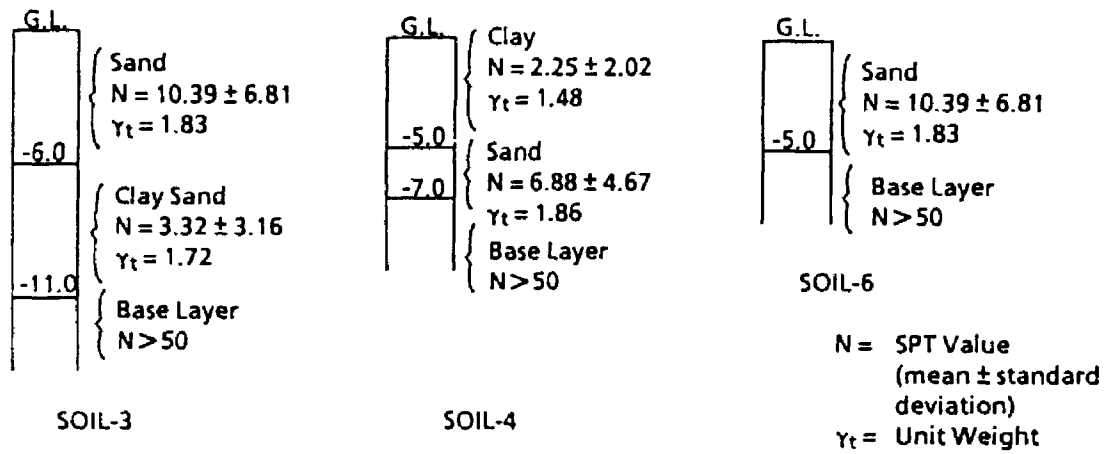


Fig.14 Fragility Curves of Liquefaction for the Soil Profiles in the Selected Area